Electrical Engineering (2021) 103:1473–1482
https://doi.org/10.1007/s00202-020-01178-1

ORIGINAL PAPER

Improvement of the induction motor sensorless control based on the type-2 fuzzy logic

Idriss Benlaloui[1,2] · Larbi Chrifi-Alaoui[3] · Mohammed Ouriagli[4] · Abderrahmane Khemis[2,5] · Dalila Khamari[2] · Said Drid[2]

Received: 22 July 2020 / Accepted: 30 November 2020 / Published online: 3 January 2021

Abstract
This paper presents MRAS speed sensorless control of induction motor using type-2 fuzzy logic controller (T2FLC). These controllers replace the PI ones, in the new MRAS strategy proposed in Benlaloui et al. (IEEE Trans Energy Convers 30(2):588–595, 2015), in order to improve the induction motor performances and robustness at low speed region. Indeed, the choice of these controllers is made because of their adaptation-based schemes which permit to handle nonlinear uncertain systems without the need of precise mathematical model required when using PI controllers. Comparative study had shown a better rejection of disturbance and high insensitivity to stator resistance compared to the PI and the T1FLC controllers. The effectiveness of the proposed speed-based T2FLC estimation method and its good robustness are validated by simulation and by experimental results.

Keywords Induction machines (IM) · Model Reference Adaptive System (MRAS) · Field-oriented control · Lyapunov Theory · Type-2 Fuzzy Logic Controller (T2FLC)

List of abbreviations

MRAS	Model Reference Adaptive System
T2FLC	Type-2 Fuzzy Logic Controller
IM	Induction machines
FOC	Field-oriented control
PI	Proportional–integral
IFOC	Indirect field-oriented control
s, r	Rotor and stator indices
d, q	Direct and quadrate indices for orthogonal components
P	Number of pairs poles
Ω	Rotor speed (rd/s)
ω_r	Induced rotor current frequency (rd/s)
J_{in}	Inertia
Γ	Unknown torque
*	Symbol indicating the command value
$\vec{x}^*$	Complex conjugate
R_s, R_r	Stator and rotor resistances
L_s, L_r	Stator and rotor inductances
T_s, T_r	Stator and rotor time constants ($T_{s,r}=L_{s,r}/R_{s,r}$)
σ	Leakage flux total coefficient ($\sigma=1-M^2/L_rL_s$)
M	Mutual inductance
ω	Mechanical rotor frequency (rd/s)
ω_s	Stator current frequency (rd/s)
f	Coefficient of viscous
Γ_e	Electromagnetic torque

1 Introduction

Speed sensorless induction motor (IM) applications are becoming more and more used in industry thanks to their mechanical robustness, higher reliability and to a reduction in bulk and cost [1, 2]. For several years, many speed estimators have been proposed for IM drive [1–10] and permanent magnet synchronous machine (PMSM) [11, 12]. In these last references a binary search algorithm-based phase-locked loop and a finite position set are used.

✉ Idriss Benlaloui
idrissb88@yahoo.fr; idriss.benlaloui@univguelma.dz

[1] Université 8 mai 1945, Guelma, Algeria

[2] LSPIE Laboratory, Electrical Engineering Department, University of Batna2, Fesdis, Algeria

[3] University of Picardie Jules Verne, LTI (EA, 3899), 13 av F. Mitterrand, 02880 Cuffies, France

[4] Laboratory of Engineering Sciences (LSI), University of Sidi Mohamed Benabdellah, Fez, Morocco

[5] University of Khenchela, EI-Hamma, Algeria

The obtained results are satisfactory, and the performances of estimators are good.

However, thanks to its simplicity, MRAS-based rotor flux [3, 13–15] remains the most applied strategy. The speed MRAS observer has been widely used in the vector control of induction motors due to its good performance and its simple structure [3, 13–15]. However, in some applications the MRAS observer may not meet the concerned robustness under parameter variations such as rotor and stator resistances and external load disturbances especially at low and zero speed regions. Therefore, many studies have been made in order to overcome this problem which remains one of the most interesting issues to be solved [16–21].

Among them, the new MRAS speed observer is proposed in [21]. Indeed, in this strategy, although PI controllers were used, the results were satisfactory. However, the use of PI controllers requires precise mathematical model, fine tuning of proportional (K_p) and integral (K_i) gain values to achieve good performance drive. However, the lack of knowledge about the actual values of some time varying parameters, such as rotor and stator resistances, limits the use of this kind of controllers. In order to overcome these drawbacks, fuzzy logic and neuro-fuzzy-based controllers were proposed [22–27]. In [22], a comparative study between a fuzzy speed controller and conventional PI controller confirms that the first one leads to advanced performance for all the operating range, such as step variation in speed. Equivalently, fuzzy speed controller in indirect field-oriented control (IFOC) technique is used in [23]. By replacing the conventional PIs in the vector control by fuzzy controllers, the trajectory tracking and the response time are improved. The use of a fuzzy regulator and a neuro-fuzzy in [24–27] for the speed control shows very satisfactory performance for all the operating range.

This paper aims to improve both the robustness and the stability of the MRAS observer especially for low speed regions by replacing conventional PIs with type-2 FLC. Indeed, the choice of these controllers is made because of their adaptation-based schemes which permit to handle nonlinear uncertain systems without the need of precise mathematical model required when using PI controllers. The type-2 fuzzy membership function takes into account uncertainties, while the type-1 fuzzy membership function does not [28].

This paper is organized as follows: In Sect. 2, the mathematical model and the vector control strategy of the induction motor are given. Then, an improved MRAS speed observer is shown in Sect. 3 and its stability is proven using Lyapunov theory. Section 4 details the principle of the proposed T2FLC algorithm. Finally, the results obtained by simulation and confirmed by experimental tests are presented in Sects. 5 and 6.

2 Vector control strategy

The voltage equations in the synchronous frame are given by:

$$\begin{cases} \bar{u}_s = R_s\bar{I}_s + \sigma L_s\dfrac{d\bar{I}_s}{dt} + \dfrac{M}{L_r}\dfrac{d\bar{\phi}_r}{dt} + j\sigma L_s\omega_s\bar{I}_s + j\dfrac{M}{L_r}\omega_s\bar{\phi}_r \\ 0 = \dfrac{1}{T_r}\bar{\phi}_r - \dfrac{M}{T_r}\bar{I}_s + \dfrac{d\bar{\phi}_r}{dt} + j\omega_r\bar{\phi}_r \end{cases} \tag{1}$$

The mechanical equation is expressed by:

$$\Gamma_e - \Gamma_l = J_{in}\frac{d\Omega}{dt} + f\Omega. \tag{2}$$

The equation of electromagnetic torque is as follows:

$$\Gamma_e = \frac{PM}{L_r}\left(I_{sq}\varphi_{rd} - I_{sd}\varphi_{rq}\right) \tag{3}$$

If we admit that the viscous coefficient and the load are not known, Eq. (2) can be written as:

$$\Gamma_e - \Gamma = J_{in}\frac{d\Omega}{dt}, \tag{4}$$

with $\Gamma = \Gamma_l + f\Omega$.

This strategy of control leads to ensure the decoupling between flux and torque [20, 21].The flux component is oriented to coincide with the axis (d), so that the following results are obtained:

$$\begin{cases} \varphi_{rq} = 0 \\ \varphi_{rd} = \varphi_r. \end{cases} \tag{5}$$

Using (5), the relations between torque, flux and current can be expressed by:

$$\Gamma_e = k_c\varphi_r I_{sq} \tag{6}$$

with $k_c = \frac{PM}{L_r}$ and I_{sq} plays the role of a control variable for the torque.

3 Improved MRAS observer

Figure 1 represents the basic configuration of MRAS approach based on adaptive model theory with reference model [20, 21].

The reference and adaptive model equations expressed in the fixed reference frame (α, β) are given, respectively, by:

$$\bar{\phi}_r = \frac{\sigma L_s L_r}{M}\bar{i}_s + \frac{L_r}{M}\int(\bar{u}_s - R_s\bar{i}_s)\,dt \tag{7}$$

$$\hat{\bar{\phi}}_r = \int\left(\frac{M}{T_r}\bar{i}_s - \left(\frac{1}{T_r} - jP.\hat{\Omega}\right)\hat{\bar{\phi}}_r\right)dt. \tag{8}$$

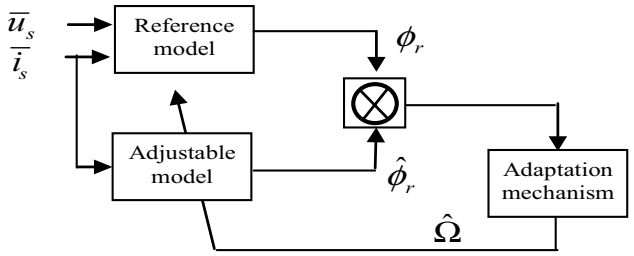

Fig. 1 Basic configuration of MRAS speed observer

The adaptation mechanism can be obtained by Lyapunov's theorem, and it is easily to extract it from Popov's criterion:

$$\int_0^t e_\varphi^T W \mathrm{d}\tau = \int_0^t (P\Delta\Omega\left[\, e_{\varphi\alpha} \;\; e_{\varphi\beta} \,\right] J\hat{\overline{\varphi}}_\mathrm{r})\mathrm{d}\tau \geq -\delta_o^2 \tag{9}$$

A low pass filter is suggested in the adaptation law to give a good speed estimation response [14]:

$$\hat{\Omega} = k_p(\overline{\varphi}_\mathrm{r} \otimes \hat{\overline{\varphi}}_\mathrm{r}) + k_i \int (\overline{\varphi}_\mathrm{r} \otimes \hat{\overline{\varphi}}_\mathrm{r})\mathrm{d}t \tag{10}$$

where k_p and k_i are positives.

However, the major disadvantage of the MRAS observer is poor performance for low speeds and sensitivity to parametric variations. Several authors have proposed different approaches to maintain performances at satisfactory level for low speed; among these solutions in [21], the speed is estimated by the use of two differences between fluxes and torques.

As, the electromagnetic torque can be described by:

$$\Gamma_e = P\frac{M}{L_\mathrm{r}}(\bar{i}_\mathrm{s} \otimes \overline{\varphi}_\mathrm{r}) \tag{11}$$

where $\overline{\varphi}_r$ is expressed by Eq. (7).

Therefore, the estimated electromagnetic torque can be described by:

$$\hat{\Gamma}_e = P\frac{M}{L_\mathrm{r}}(\bar{i}_\mathrm{s} \otimes \hat{\overline{\varphi}}_\mathrm{r}) \tag{12}$$

where $\hat{\overline{\phi}}_\mathrm{r}$ is expressed by Eq. (8).

It can be easily demonstrated that according to the equation of motion (2) each variation of the load torque causes a variation of the speed and consequently the estimated variation of the speed is exactly equal to the estimated variation of the electromagnetic torque.

Then, we replace the electromagnetic torque and the speed by their estimated values in the motion Eq. (2); we obtain:

$$\hat{\Gamma}_e - \Gamma_l = J_\mathrm{in}\frac{\mathrm{d}\hat{\Omega}}{\mathrm{d}t} + f\hat{\Omega}. \tag{13}$$

We obtain Eq. (14) by the subtraction of (13) from (2)

$$e_\Gamma = \Gamma_e - \hat{\Gamma}_e = J_\mathrm{in}\frac{\mathrm{d}(\Omega - \hat{\Omega})}{\mathrm{d}t} + f(\Omega - \hat{\Omega}). \tag{14}$$

To ensure a good estimate, the following two conditions must be taken into account:

$$\begin{cases} \dot{\bar{e}}_\phi = -\left(\dfrac{1}{T_r} - jP\Omega\right)\bar{e}_\phi + jP\left(\Omega - \hat{\Omega}\right)\hat{\bar{\phi}}_r \\ e_\Gamma = \Gamma_e - \hat{\Gamma}_e = J_\mathrm{in}\dfrac{\mathrm{d}(\Omega - \hat{\Omega})}{\mathrm{d}t} + f(\Omega - \hat{\Omega}). \end{cases} \tag{15}$$

By following the same reasoning with which the adaptation law has been determined and taking into account the torque adaptation error, the speed adaptation law becomes:

$$\hat{\Omega} = \left(K_\mathrm{p} + \frac{K_\mathrm{i}}{p}\right)(\overline{\phi}_\mathrm{r} \otimes \hat{\overline{\phi}}_\mathrm{r}) + K_\Gamma\frac{e_\Gamma}{\tau p + 1}, \tag{16}$$

where τ is chosen to be close to the mechanical time constant.

In this approach, the electromagnetic torque error is filtered by a low pass filter and added to the conventional adaptation law loop. The diagram of the new MRAS estimator is shown in Fig. 2.

4 Design of type-2 fuzzy logic controller

In order to achieve a high dynamic performance of the new MRAS approach, we replace all the conventional PI of vector control regulator and classical MRAS adaptation mechanism of rotor speed estimation by the T2FLC algorithm, which provided satisfactory solutions in [19–22]. The inputs of the proposed algorithm for new MRAS adaptation mechanism are the rotor flux static and dynamic errors $\bar{e}_\phi = (\overline{\phi}_r - \hat{\overline{\phi}}_r)$, which can be expressed as:

$$\Delta e_\phi(k) = e_\phi(k) - e_\phi(k-1) \tag{17}$$

These two inputs are multiplied by two scaling factors G_{e_φ} and $G_{\Delta e_\varphi}$, respectively. The output of the controller is multiplied by a third scaling factor G_u to generate the actual value of the rate of change of estimated rotor speed.

The three quantities, E_φ, ΔE_φ (inputs), and $\Delta\hat{\Omega}$ (output), are standardized as follows:

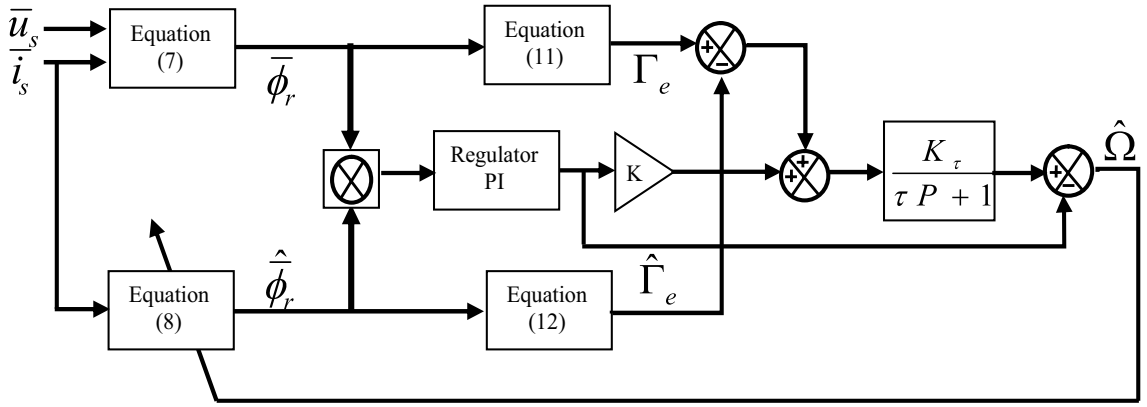

Fig. 2 The novel configuration design of MRAS

Table 1 Scale factors

Scale factor G_{i_j}	Estimated speed $\hat{\Omega}$	Torque Γ_e
$G_{e_{\varphi,\Omega}}$	100	100
$G_{\Delta e_\varphi, \Delta e_\Omega}$	1000	1000
G_u	0.9	0.9

$$\begin{cases} E_\varphi = G_{e_\varphi} e_\varphi \\ \Delta E_\varphi = G_{\Delta e_\varphi} \Delta e_\varphi \\ \Delta \hat{\Omega} = G_u \Delta \hat{\omega} \end{cases} \tag{18}$$

Therefore, the inputs of vector control regulator are the rotor speed and dynamic errors cited above which can be expressed as:

$$\Delta e_\Omega(k) = e_\Omega(k) - e_\Omega(k-1) \tag{19}$$

These two inputs are multiplied by two scaling factors G_{e_Ω} and $G_{\Delta e_\Omega}$, respectively. The output of the controller is multiplied by a third scaling factor G_u to generate the actual value of the electromagnetic torque Γ_e reference.

The three quantities, e_Ω, Δe_Ω (inputs), and $\Delta\Gamma_e$ (output), are standardized as follows:

$$\begin{cases} E_\Omega = G_{e_\Omega} e_\Omega \\ \Delta E_\Omega = G_{\Delta e_\Omega} \Delta e_\Omega \\ \Delta \Gamma'_e = G_u \Delta \Gamma_e \end{cases} \tag{20}$$

where G_{e_Ω},$G_{\Delta e_\Omega}$ and G_u are scale factors or normalization, and play an important role on the control performance. The trial-and-error technique is usually used to tune these gains to ensure optimal performance of the controller [28].

The values of scale factors are given in Table 1.

Finally, a discrete integration is performed to get the value of the estimated speed and electromagnetic torque reference Γ_e. Hence, FLC is designed as shown in Figs. 3, 4, 5 and 6. The expressions of the estimated speed and electromagnetic torque reference can be written as:

$$\hat{\Omega}(k) = \hat{\Omega}(k-1) + G_u \Delta \hat{\Omega}(k) \tag{21}$$

$$\Gamma_e(k) = \Gamma_e(k-1) + G_u \Delta \Gamma_e(k) \tag{22}$$

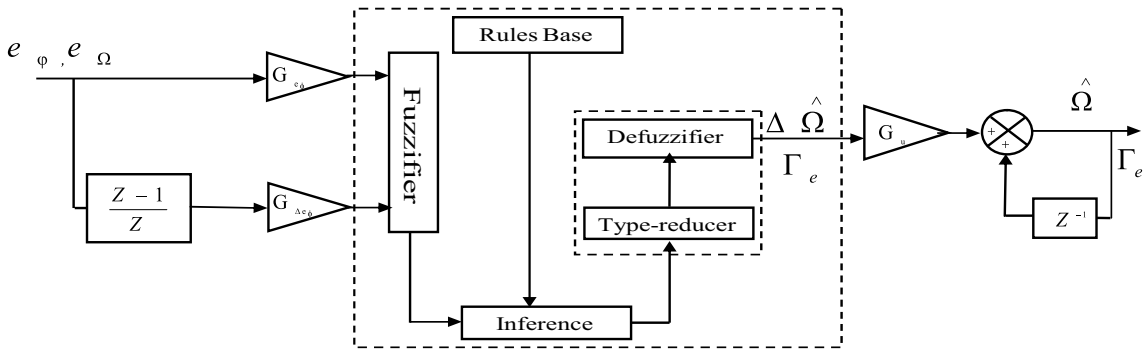

Fig. 3 Proposed type-2 fuzzy logic controllers

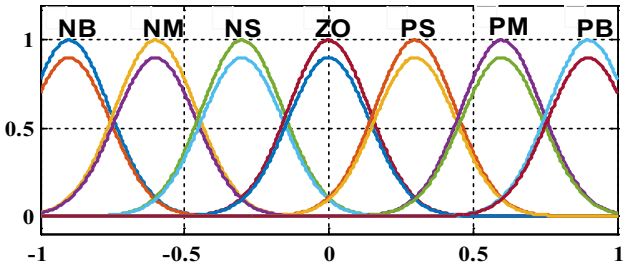

Fig. 4 Fuzzy type-2 membership functions for error variation flux and rotor speed

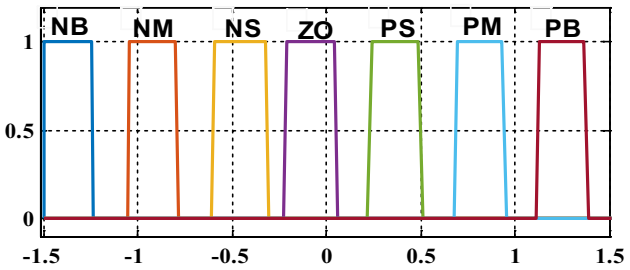

Fig. 5 Fuzzy type-2 membership functions for estimated speed

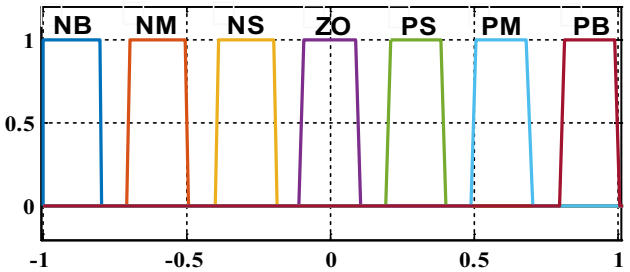

Fig. 6 Fuzzy type-2 membership for reference electromagnetic torque

The type-2 membership functions of errors (e_ϕ, e_Ω) and variation errors ($\Delta e_\phi, \Delta e_\Omega$) of flux and rotor speed are chosen identical with Gaussian forms and are defined on the interval $[-1\ ,\ 1]$ (Fig. 4). The type-2 belonging functions of the variation Γ_e and $\hat{\Omega}$ are chosen with intervals form on the interval $[-1.5\ ,\ 1.5]$ (Fig. 5), and the variation $\Delta\hat{\Omega}$ is chosen with intervals form on the interval (Fig. 6).

In Figs. 7 and 8, we present the block diagrams of the new MRAS observer and the general scheme of the proposed control.

5 Simulation and experimental results

In what follows, the simulation and experimental results best embody the performance of the proposed observer structure. First, the performances of the proposed approach with PI and T2FLC are analyzed and compared by simulation. Second, dSPACE DS 1104 was used to validate the simulation results through extensive experimentations.

The values of all controllers' gains, and the rating and parameters of the induction motor are listed in Table 1 and in "Appendix," respectively.

5.1 Simulation results

In order to demonstrate the efficiency of the control structure, a sensorless field-oriented controlled induction motor drive, as shown in Fig. 8 is used. Full nonlinear simulations were carried out for the speed and for load torque variation (Figs. 9, 10, 11, 12 and 13).

Figures 10 and 11 represent responses of the actual rotor speed and the estimated one following the specified reference. We can see in Figs. 11, 12 and 13 a fast convergence toward zero of speed estimation error and that of

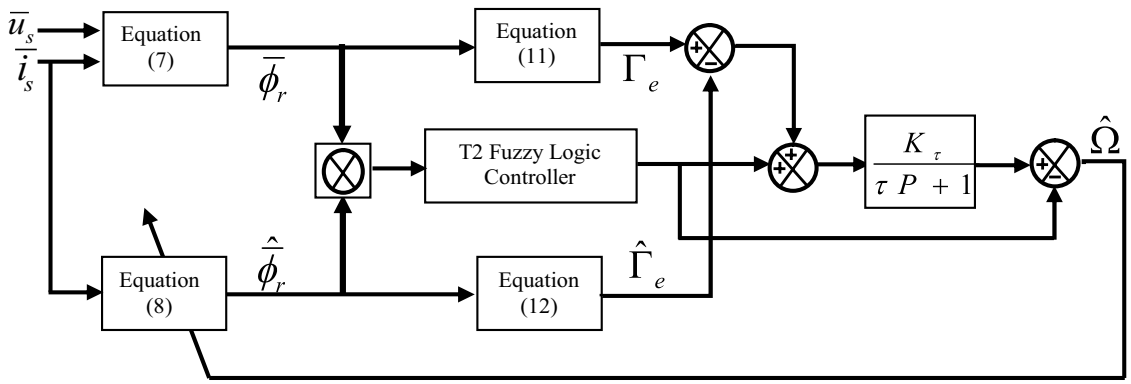

Fig. 7 Block diagram of MRAS speed observer with T2FLC

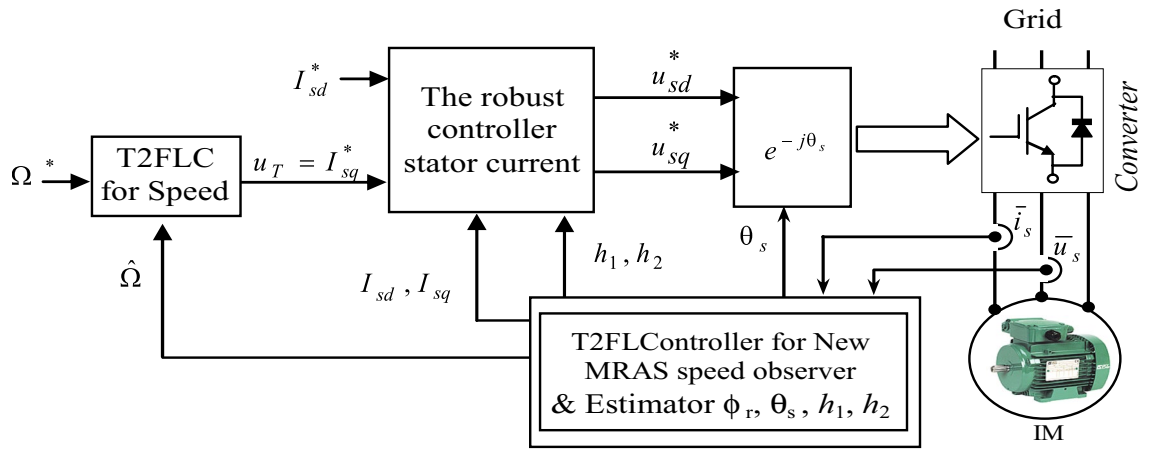

Fig. 8 General scheme of the proposed control

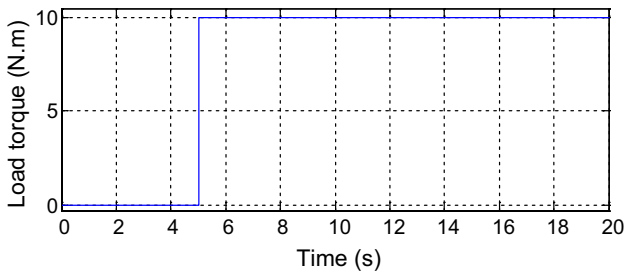

Fig. 9 Load torque variation

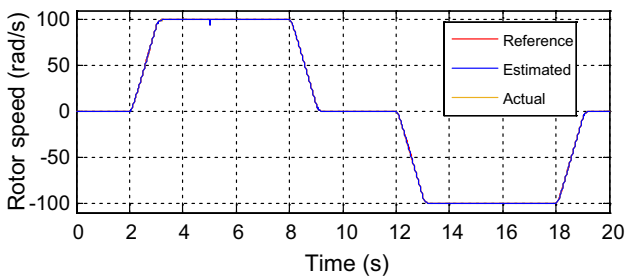

Fig. 10 Speed of induction motor

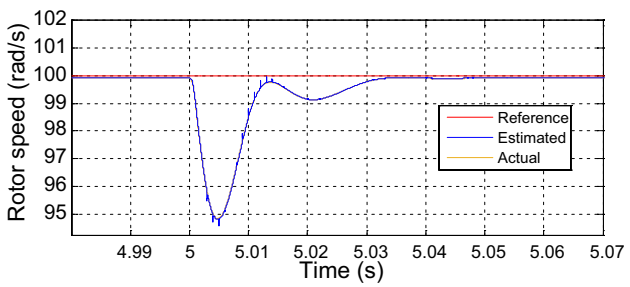

Fig. 11 Zoom of reference, actual and estimated rotor speed

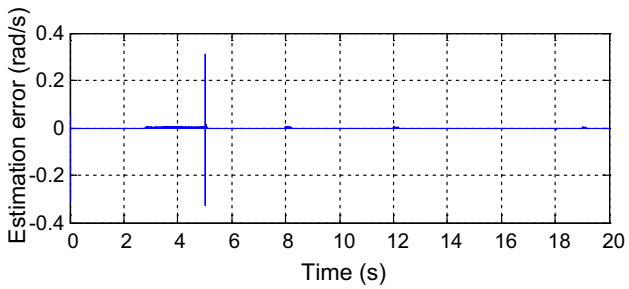

Fig. 12 Speed estimation error

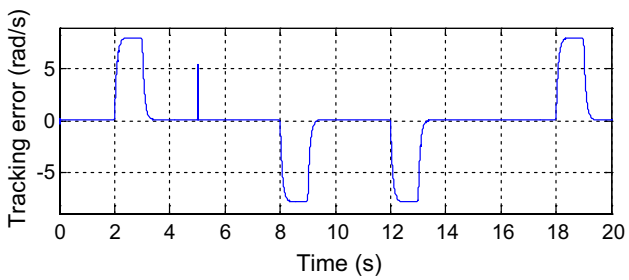

Fig. 13 Speed tracking error

the tracking; also, estimated speed is very satisfactory at zero regions. A robustness test for a load torque variation at a constant speed reference shows the efficiency of the type-2 FLC, where a step load variation of 10 Nm (Fig. 9) is applied at $t = 5$ s. In addition, in order to confirm the field orientation, d and q axis fluxes are separately shown in Fig. 14.We can see that the q axis flux is maintained at zero value. In Fig. 15, we can see the influence of the load variation on the I_{sq} current at $t = 5$ s and on the other hand no effect on the direct current I_{sd} of the machine. Figures 16 and 17 show that the current peaks remain within acceptable limits.

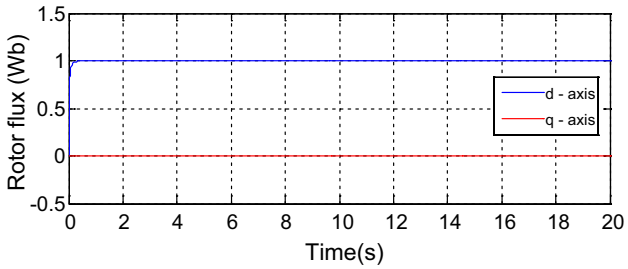

Fig. 14 Rotor flux

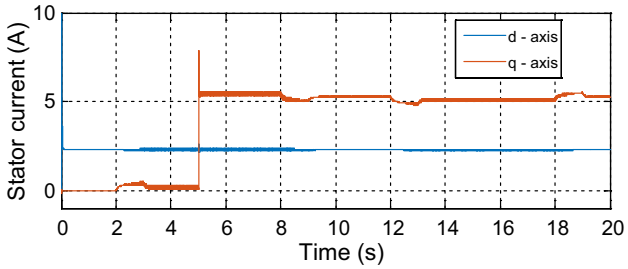

Fig. 15 I_{sd} and I_{sq} stator currents

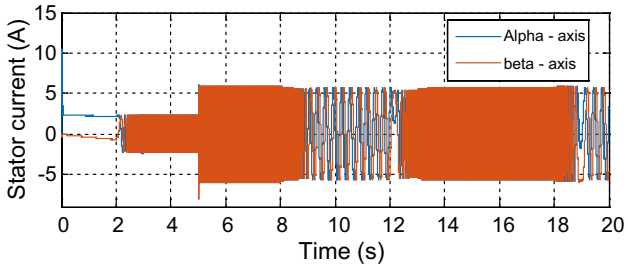

Fig. 16 $I_{s\alpha}$ and $I_{s\beta}$ stator currents

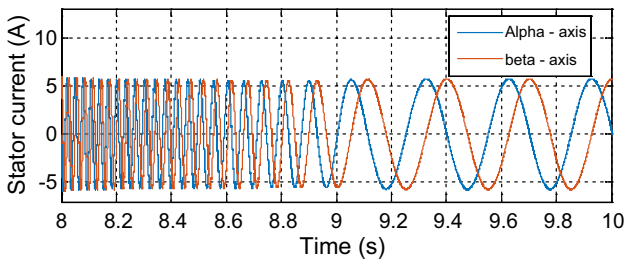

Fig. 17 Zoom of $I_{s\alpha}$ and $I_{s\beta}$ stator currents

5.2 Description of the laboratory setup

Experimental tests are conducted by using dSPACE DS1104 to implement the novel proposed analysis and design approach of rotor MRAS speed observer. Figure 18 shows the basic structure of the laboratory setup with all its parts. The IM stator is fed by a converter under direct control of the DS1104 board. In order to measure the mechanical speed, the encoder is used. The sensors used for the currents and voltages measure are LA-55NP and LV-25P, respectively. The DS1104 PPC controller connected signals are provided galvanic isolation with the Interface.

5.3 Experimental results

Figure 20 shows estimated, actual and reference speeds. As we can see in Figs. 19 and 20 that despite of the load torque at $t=5$ s speed estimation and tracking errors are small and converge swiftly to zero. We also notice, as can be seen in Fig. 21, that the current i_{sd} is kept constant for all the operating range. Figures 22, 23, 24 and 25 show that the stator voltage and current phase are maintained at their rate value. This proves the efficiency proposed control.

In order to confirm the performances of the new control structure at low speed regions respect to load torque and stator resistance R_s variations, a load torque of 10 Nm and $+20\%R_s$ variations are applied to the motor at $t=3.5$ s and $t=6.6$, respectively; it is clearly shown in Figs. 26 and 27 that the new structure with T2FLC controller is capable to provide a quick response and a better rejection of disturbance. Then, it confirms the insensitivity to stator resistance of the speed response.

6 Comparative study between PI, T1FL and T2FL controllers

In order to confirm the performances of the new control structure using T2FLC, a comparison between simulation results obtained at low speed regions by T2FLC, classical PI and T1FLC controllers was carried out with respect to load torque and stator resistance variations. A load torque of 10 Nm and $+30\%R_s$ variations are applied to the motor at $t=5$ s and $t=7$ s, respectively. It is clearly shown in Figs. 28 and 29 that the new structure with T2FLC controller is able to provide a quick response, a better rejection of disturbance and high insensitivity to stator resistance compared to the PI and the T1FLC controllers.

Also comparative study between T2FLC and T1FLC was made by using the performance indexes, integral squared error (**ISE**), integral absolute error (**IAE**) and the integral of time multiplied absolute error (**ITAE**) as given in [25].

The results of the study are given in Table 2.

As can be seen, these results confirm the improved performance of the type-2 fuzzy logic controller.

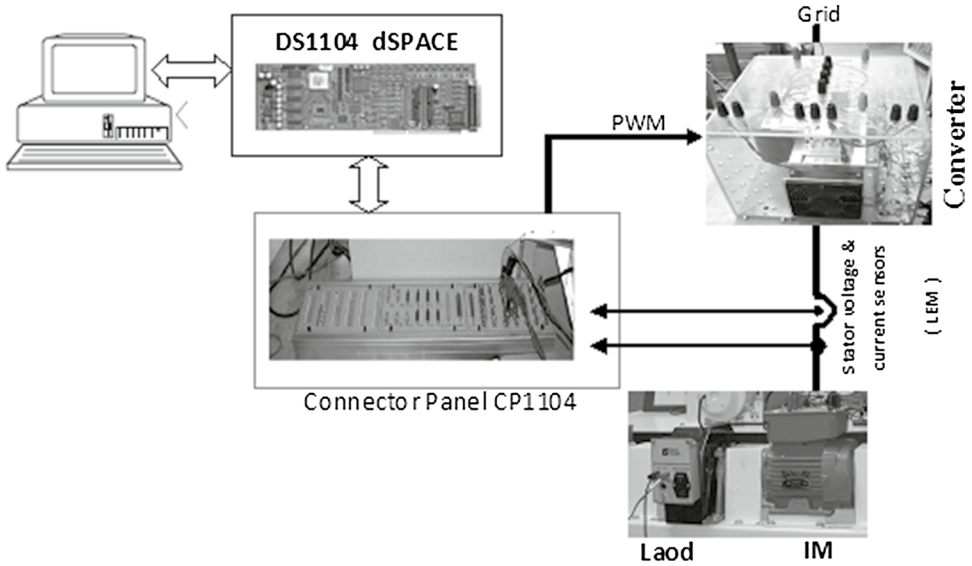

Fig. 18 Structure of the laboratory setup

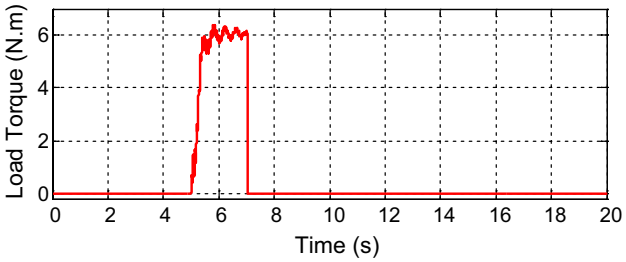

Fig. 19 Load torque variation

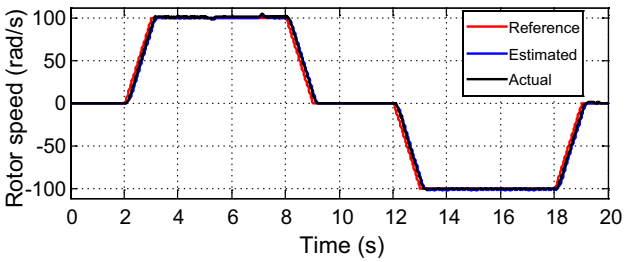

Fig. 20 Speed of induction motor

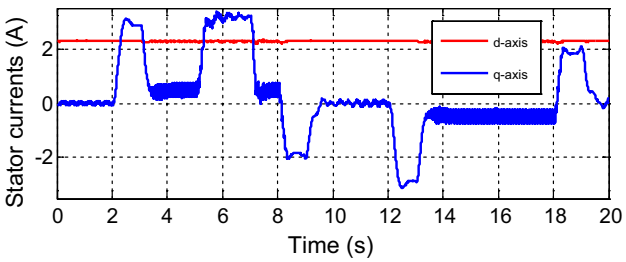

Fig. 21 I_{sd} and I_{sq} stator currents

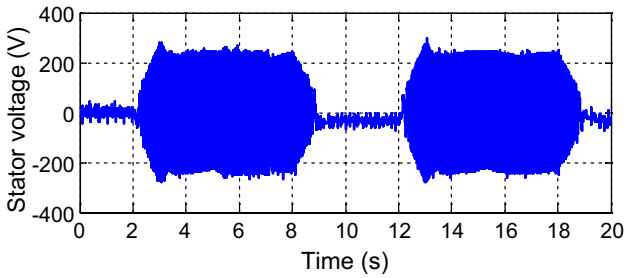

Fig. 22 The stator phase voltage

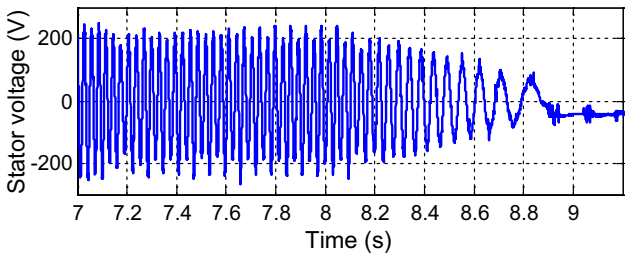

Fig. 23 Zoom of the stator phase voltage

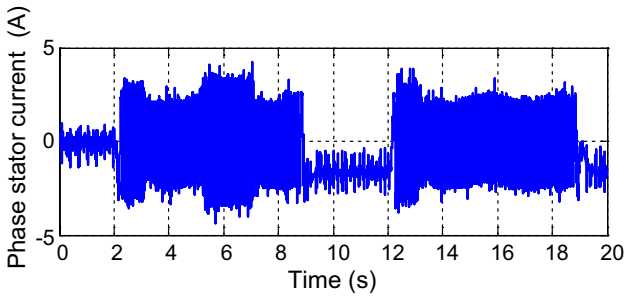

Fig. 24 The stator phase current

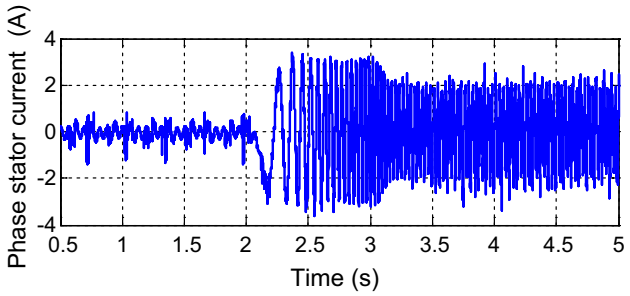

Fig. 25 Zoom of the stator phase current

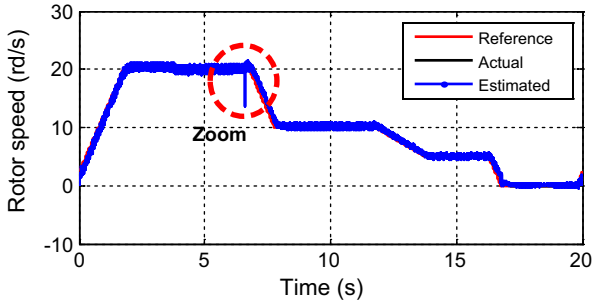

Fig. 26 Rotor speed

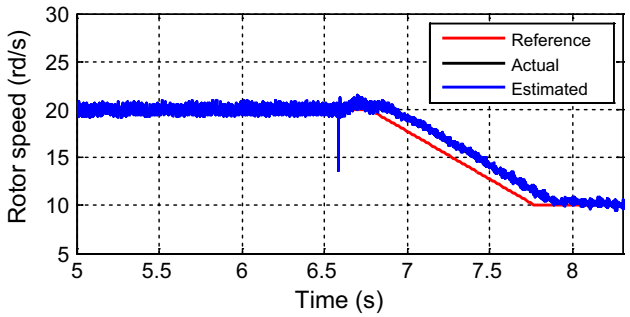

Fig. 27 Zoom of rotor speed

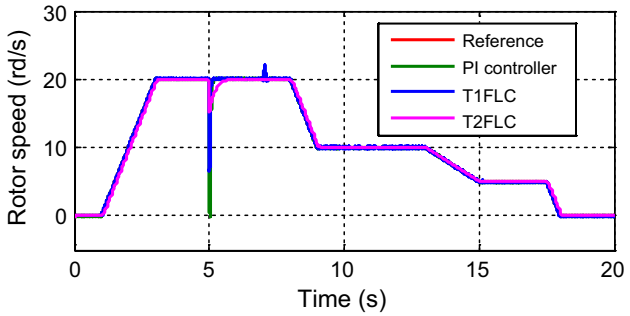

Fig. 28 Rotor speed response with T2FLC, T1FLC and PI controllers

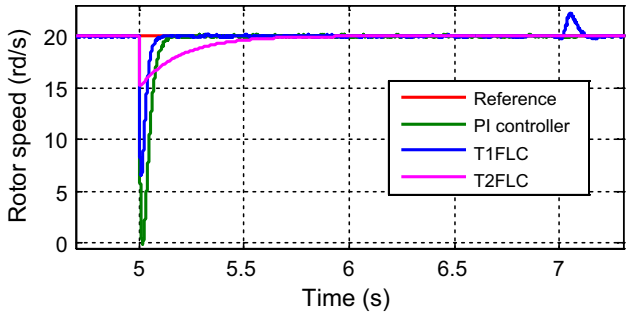

Fig. 29 Zoom of rotor speed response with T2FLC, T1FLC and PI controllers

Table 2 Performance indexes

	Rotor speed estimated (rad/s)	
	Fuzzy type 1	Fuzzy type 2
IAE	0.3155	0.05393
ISE	1.491	0.1176
ITAE	10.35	0.8214

7 Conclusions

In this paper, we have presented an improved MRAS T2FLC controller and observer for sensorless rotor speed control of induction machine. When the conventional PI has been replaced by type-2 fuzzy logic controllers, simulation and experimental results showed a clear improvement in performance regarding robustness with respect to load torque and stator resistance variations, compared with classical PI and fuzzy logic type-1 controller-based method. The simulation and experimental results reveal and demonstrate high performances of the induction motor control.

Appendix

Machine parameters and rated values

$R_r = 5.1498\ \Omega$; $R_s = 12.75\ \Omega$; $M = 0.4331$ H; $L_s = 0.4991$ H; $L_r = 0.4331$ H; $J = 0.0035$ kg m^2; $f = 0.001$ Nm s/rd; $Pn = 0.9$ kW; $n = 1400$ rpm; $p = 2$; $f = 50$ Hz; load torque = 10 Nm.

References

1. Ha J-I, Sul S-K (1999) Sensorless field-orientation control of an induction machine by high-frequency signal injection. IEEE Trans Ind Appl 35(1):45–51. https://doi.org/10.1109/28.740844

2. Maiti S, Chakraborty C, Hori Y, Ta MC (2008) Model reference adaptive controller-based rotor resistance and speed estimation techniques for vector controlled induction motor drive utilizing reactive power. IEEE Trans Ind Electron 55(2):594–601. https://doi.org/10.1109/TIE.2007.911952
3. Comanescu M, Xu L (2006) Sliding-mode MRAS speed estimators for sensorless vector control of induction machine. IEEE Trans Ind Electron 53(1):146–153. https://doi.org/10.1109/TIE.2005.862303
4. Ravi Teja AV, Verma V, Chakraborty C (2015) A new formulation of reactive-power-based model reference adaptive system for sensorless induction motor drive. IEEE Trans Ind Electron 62(11):6797–6808. https://doi.org/10.1109/TIE.2015.2432105
5. Zorgani YA, Koubaa Y, Boussak M (2016) MRAS state estimator for speed sensorless ISFOC induction motor drives with Luenberger load torque estimation. ISA Trans 61:308–317. https://doi.org/10.1016/j.isatra.2015.12.015
6. Das S, Kumar R, Pal A (2019) MRAS-based speed estimation of induction motor drive utilizing machines' d- and q-circuit impedances. IEEE Trans Ind Electron 66(6):4286–4295. https://doi.org/10.1109/TIE.2018.2860530
7. Kumar R, Das S, Bhaumik A (2019) Speed sensorless model predictive current control of doubly-fed induction machine drive using model reference adaptive system. ISA Trans 86:215–226. https://doi.org/10.1016/j.isatra.2018.10.025
8. Dehghan-Azad E, Gadoue S, Atkinson D, Slater H, Barrass P, Blaabjerg F (2018) Sensorless control of IM based on stator-voltage MRAS for limp-home EV applications. IEEE Trans Power Electron 33(3):1911–1921. https://doi.org/10.1109/TPEL.2017.2695259
9. Korzonek M, Tarchala G, Orlowska-Kowalska T (2019) A review on MRAS-type speed estimators for reliable and efficient induction motor drives. ISA Trans 93:1–13. https://doi.org/10.1016/j.isatra.2019.03.022
10. Sun X, Chen L, Yang Z, Zhu H (2013) Speed-sensorless vector control of a bearingless induction motor with artificial neural network inverse speed observer. IEEE/ASME Trans Mechatron 18(4):1357–1366. https://doi.org/10.1109/tmech.2012.2202123
11. Sun X, Hu C, Lei G, Yang Z, Guo Y, Zhu J (2020) Speed sensorless control of SPMSM drives for EVs with a binary search algorithm-based phase-locked loop. IEEE Trans Veh Technol 69:4968–4978. https://doi.org/10.1109/tvt.2020.2981422
12. Sun X, Cao J, Lei G, Guo Y, Zhu J (2020) Speed sensorless control for permanent magnet synchronous motors based on finite position set. IEEE Trans Ind Electron 67(7):6089–6100. https://doi.org/10.1109/tie.2019.2947875
13. Hinkkanen M, Luomi J (2003) Modified integrator for voltage model flux estimation of induction motors. IEEE Trans Ind Electron 50(4):818–820. https://doi.org/10.1109/TIE.2003.814996
14. Pal A, Das S, Chattopadhyay AK (2018) An improved rotor flux space vector based MRAS for field-oriented control of induction motor drives. IEEE Trans Power Electron 33(6):5131–5141. https://doi.org/10.1109/TPEL.2017.2657648
15. Smith AN, Gadoue SM, Finch JW (2016) Improved rotor flux estimation at low speeds for torque MRAS-based sensorless induction motor drives. IEEE Trans Energy Convers 31(1):270–282. https://doi.org/10.1109/TEC.2015.2480961
16. Rashed M, Stronach AF (2004) A stable back-EMF MRAS-based sensorless low-speed induction motor drive insensitive to stator resistance variation. IEE Proc Electr Power Appl 151(6):685. https://doi.org/10.1049/ip-epa:20040609
17. Zaky MS, Khater MM, Shokralla SS, Yasin HA (2009) Wide-speed-range estimation with online parameter identification schemes of sensorless induction motor drives. IEEE Trans Ind Electron 56(5):1699–1707. https://doi.org/10.1109/TIE.2008.2009519
18. Huang S, Wang Y, Gao J, Lu J, and Qiu S (2004) The vector control based on MRAS speed sensorless induction motor drive. In: Fifth world congress on intelligent control and automation (IEEE Cat. No. 04EX788), 5: 4550–4553. https://doi.org/10.1109/wcica.2004.1342378
19. Karanayil B, Rahman MF, Grantham C (2004) An implementation of a programmable cascaded low-pass filter for a rotor flux synthesizer for an induction motor drive. IEEE Trans Power Electron 19(2):257–263. https://doi.org/10.1109/TPEL.2003.823181
20. Benlaloui I, Drid S, Khamari D, Chrifi-Alaoui L, Marhic B, and Ouriagli M (2016) Analysis and design of rotor MRAS speed sensorless with a novel approach. In: 2016 17th International conference on sciences and techniques of automatic control and computer engineering (STA) 4:73–77. https://doi.org/10.1109/STA.2016.7952016
21. Benlaloui I, Drid S, Chrifi-Alaoui L, Ouriagli M (2015) Implementation of a new MRAS speed sensorless vector control of induction machine. IEEE Trans Energy Convers 30(2):588–595. https://doi.org/10.1109/STA.2016.7952016
22. Hakju L, Jaedo L, and Sejin S (2001) Approach to fuzzy control of an indirect field-oriented induction motor drives. In: ISIE 2001. 2001 IEEE international symposium on industrial electronics proceedings (Cat. No. 01TH8570) 2(1):1119–1123. https://doi.org/10.1109/ISIE.2001.931633
23. Badr BM, Eltamaly AM, Alolah AI (2010) Fuzzy controller for three phases induction motor drives. IEEE Veh Power Propuls Conf 2010:1–6. https://doi.org/10.1109/VPPC.2010.5729080
24. Khemis A, Benlaloui I, Drid S, Chrifi-Alaoui L, Khamari D, Menacer A (2018) High-efficiency induction motor drives using type-2 fuzzy logic. Eur Phys J Plus 133(3):86. https://doi.org/10.1140/epjp/i2018-11903-6
25. Ramesh T, Kumar Panda A, Shiva Kumar S (2015) Type-2 fuzzy logic control based MRAS speed estimator for speed sensorless direct torque and flux control of an induction motor drive. ISA Trans 57:262–275. https://doi.org/10.1016/j.isatra.2015.03.017
26. Phukon LJ, Baruah N (2015) Design of fuzzy logic controller for performance optimisation of induction motor using indirect. Int J Electr Electron Data Commun 3(2):72–78
27. Rashed Mohan Krishna S, Febin Daya JL (2016) MRAS speed estimator with fuzzy and PI stator resistance adaptation for sensorless induction motor drives using RT-lab. Perspect Sci 8:121–126. https://doi.org/10.1016/j.pisc.2016.04.013
28. Hong Y-Y, Buay PMP (2020) Robust design of type-2 fuzzy logic-based maximum power point tracking for photovoltaics. Sustain Energy Technol Assess 38:100669. https://doi.org/10.1016/j.seta.2020.100669